

# Effect of metal decoration on sulfur-based gas molecules adsorption on phosphorene

**Yonghu Wang**

Key Laboratory of Microelectromechanical Systems of the Ministry of Education, Southeast University, Nanjing 210096

**Shuangying Lei** (✉ [lsy@seu.edu.cn](mailto:lsy@seu.edu.cn))

Key Laboratory of Microelectromechanical Systems of the Ministry of Education, Southeast University, Nanjing 210096

**Ran Gao**

Key Laboratory of Microelectromechanical Systems of the Ministry of Education, Southeast University, Nanjing 210096

**Xiaolong Sun**

Key Laboratory of Microelectromechanical Systems of the Ministry of Education, Southeast University, Nanjing 210096

**Jie Chen**

Key Laboratory of Microelectromechanical Systems of the Ministry of Education, Southeast University, Nanjing 210096

---

## Research Article

**Keywords:** Density functional theory, Sulfur-based gas molecules, Metal-decorated Phosphorene

**Posted Date:** March 3rd, 2021

**DOI:** <https://doi.org/10.21203/rs.3.rs-109436/v2>

**License:**   This work is licensed under a Creative Commons Attribution 4.0 International License. [Read Full License](#)

---

# Abstract

Using the first-principles calculation based on density functional theory (DFT), we systematically studied the adsorption of sulfur-based gas molecules ( $\text{H}_2\text{S}$ ,  $\text{SO}_2$ ,  $\text{SO}_3$ ) on various metal-decorated phosphorenes. To avoid the formation of metal clusters on the surface of phosphorene, eleven metals (Li, Na, K, Rb, Cs, Ca, Sr, Ba, Ni, La, Tl) with bulk cohesive energy less than the binding energy on the phosphorene are considered. Except for  $\text{H}_2\text{S}$  on Tl-decorated phosphorene, all metal decorations can improve the adsorption strength of phosphorene to sulfur-based gas molecules, and  $E_{\text{ads}}(\text{H}_2\text{S}) < E_{\text{ads}}(\text{SO}_2) < E_{\text{ads}}(\text{SO}_3)$  for the same metal decoration case. In addition, some metal-decorated phosphorene systems exhibit interesting magnetic and electrical changes after sulfur-based gas molecule adsorptions, indicating that these metal-decorated phosphorene systems are promising to be used for the detection and removal of sulfur-based gas molecules.

## 1. Introduction

Air pollution is becoming more and more serious with the rapid development of industrialization. Thanks to attenuation of organic substances, emission of sewage plants and burning of fossil fuels [1–4], every year more than billion tons of sulfur-based gases are discharged into the atmosphere [5, 6]. The sulfur-containing gas compounds are all dangers for human health [7–9].  $\text{SO}_2$  hurts the nerves in the respiratory system, including lesions in nasal cavity and throat.  $\text{H}_2\text{S}$  inhibits the metabolism of cells in the livers [10, 11]. In terms of environmental pollution, sulfur-containing gas compounds can bring about sulfuric acid mist, sulphate aerosol, as well as acidic soil, which further harm animals and plants [12, 13]. Therefore, the treatment of sulfur-based exhaust gases is essential.

Adsorption is great competitive in the removal and detection of sulfur-based gases. A lot of experimental and theoretical investigations on the adsorption of sulfur-based gas compounds on metal and metal oxide are performed [14–16]. However, owing to the strict operating condition and low sensitivity, the metal and metal oxide are not the ideal candidate materials for sensing the sulfur-based gas compounds [17]. On the other hand, since the discovery of graphene in 2004 [18–20], two-dimensional (2D) materials have aroused great interest of researchers owing to their superior mechanical, thermal, optical and electronic properties [21–24]. Another striking feature of 2D materials is the large surface-to-volume ratio, which may be attractive for gas detection and adsorption. Recently, the researchers uncovered that phosphorene has an advantage over graphene on the adsorption of small molecule gases because of its puckered surface morphology and higher surface-to-volume ratio [25, 26]. Both theoretical and experimental researches have proven that phosphorene possesses the excellent gas sensing sensitivity [27, 28]. However, the adsorption energies of gas molecules on pristine phosphorenes are too small, hence the surface decoration or/and doping is demanded to enhance the adsorption of gas molecules [29–31]. For sulfur-based gas adsorption on phosphorene, the adsorptions of defective and metal substitute doped phosphorenes to  $\text{H}_2\text{S}$  and  $\text{SO}_2$  were investigated by Kaewmaraya, which exposed that metal-dopings could significantly enhance the adsorption of phosphorene to  $\text{SO}_2$  [32].

In this manuscript, we have systematically studied the adsorption of sulfur-based gas molecules ( $\text{H}_2\text{S}$ ,  $\text{SO}_2$ ,  $\text{SO}_3$ ) on various metal-decorated phosphorene by using the first-principles calculation. To avoid clustering of metals on the surface of phosphorene, eleven metals have been opted on the basis of their bulk cohesive energy less than the binding energy. They are alkali (Li, Na, K, Rb, Cs), alkaline earth (Ca, Sr), transition (Ni, La), and post-transition (Tl) metals. Except for  $\text{H}_2\text{S}$  on Tl-decorated phosphorene, all metal decorations can improve the adsorption of sulfur-based gas molecules on phosphorene, especially Ni/Al-decorated phosphorene. In addition, some metal-decorated phosphorene systems exhibit interesting magnetism and electrical transitions after  $\text{SO}_2$  and  $\text{SO}_3$  gas molecules adsorption, which could have potential application for  $\text{SO}_2$  and  $\text{SO}_3$  gas detection.

## 2. Computational Methods

In this article, all the density functional theory (DFT) calculations have been carried out by the Vienna ab initio simulation software package code (VASP) [33, 34]. We took advantage of the Perdew-Burke-Ernzerhof (PBE) functional of generalized gradient approximation (GGA) to describe exchange-correlation interaction [35]. The van der Waals (vdW) interactions were dealt with by adopting empirical correction scheme of Grimme (DFT+D3) [36]. In all the calculations, the kinetic energy cut-off for the plane-wave basis was 500 eV. The 3×4 supercells and the vacuum distances of 15 Å were utilized to reduce the interaction of mirror adsorbates and phosphorene layers, respectively, and the corresponding *k*-point grids were set as 3×3×1 by Monkhorst-Pack *k*-point scheme. The energy convergence accuracy was set to 10<sup>-5</sup> eV, and all the structures were fully relaxed until the forces acting upon each atom were less than 0.01 eV/Å. For sulfur-based gas molecules adsorption on pristine phosphorene or metal-decorated phosphorene, the adsorption energy (*E*<sub>ads</sub>) is calculated by the formula, **see formula 1 in the supplementary files**.

## 3. Results And Discussion

### 3.1 Sulfur-based gas molecules adsorption on pristine phosphorene

The lattice constants of the pristine phosphorene monolayer along the armchair and zigzag directions are respectively 4.57 and 3.31 Å, and a direct bandgap is 0.88 eV, in agreement with previous studies [37, 38]. For the adsorption of sulfur-based gas molecules (H<sub>2</sub>S, SO<sub>2</sub>, SO<sub>3</sub>) on pristine phosphorene, various possible initial adsorption sites [e.g. hollow (H), bridge (B), top (T)] and adsorption configurations were considered. By comparing the total energies of the adsorption configurations after structural optimization, the most stable adsorption structures were obtained as shown in figure 1. The H<sub>2</sub>S prefers to adsorb at the hollow site with H atoms pointing to the phosphorene surface, while the SO<sub>2</sub> and SO<sub>3</sub> prefer to adsorb at the T site lying parallel to the phosphorene surface. The nearest atom-to-atom distances between H<sub>2</sub>S, SO<sub>2</sub> and SO<sub>3</sub> molecules and the surface of the phosphorene are 2.818, 2.984 and 2.572 Å, respectively. The adsorption energies of H<sub>2</sub>S, SO<sub>2</sub> and SO<sub>3</sub> on phosphorene are calculated by using Eq (1), as 0.220, 0.396 and 0.646 eV respectively. To analyze the intrinsic mechanism of interaction between sulfur-based gas molecules and phosphorene, the differential charge density (DCD) of the most stable adsorption configurations were calculated, as illustrated in figure 1(d)-(f). It can be seen that, from H<sub>2</sub>S to SO<sub>2</sub> to SO<sub>3</sub>, the electron accumulations around gas molecules increase significantly, which are also confirmed by the Bader charge analysis. The Bader charge analysis shows that the electrons transferred from the phosphorene to H<sub>2</sub>S, SO<sub>2</sub> and SO<sub>3</sub> molecules are 0.003, 0.182 and 0.451 e, respectively, ascribing to higher electronegativity of gas molecules over the phosphorene. Generally, the more charge quantities transferred means the stronger interactions, and thus the larger adsorption energies [39]. Here, the variation trend of charge quantities transferred does agree with that of the adsorption energies (see table 1).

To understand the effect of the adsorption of sulfur-based gas molecules on the electrical properties of phosphorene, the local density of states (LDOS) of the adsorption system were calculated, as shown in figure 1. In LDOSs, the DOS near the Fermi level is zero for all three adsorption systems, indicating the adsorption of sulfur-based gas molecules don't change the semiconductor properties of phosphorene. The bandgaps of phosphorenes are respectively 0.86 and 0.87 eV after H<sub>2</sub>S and SO<sub>2</sub> adsorptions, which are marginally smaller than that of pristine one, while the bandgap of phosphorene slightly increase to 0.89 eV after SO<sub>3</sub> adsorption. After sulfur-based gas molecule adsorptions, the slight variations of bandgaps may be ascribed to the change of channel of phosphorene according to the definition in Ref. 40. In Ref. 40, the authors proposed that the narrower channel (3.49 for H<sub>2</sub>S and 3.44 for SO<sub>2</sub> as compared to 3.54 for pristine phosphorene) would result in the stronger repulsive interaction between the facing lone pairs at the ditch of

phosphorene and thus the decrease of bandgap, and vice versa. For H<sub>2</sub>S adsorption case, the H atom is the nearest to the P atom, but the H atomic DOS is far from the Fermi level, which should be also responsible for the smaller adsorption energy. In the case of SO<sub>2</sub> and SO<sub>3</sub>, the S atoms are the closest to P atoms. Near Fermi levels, the S DOS peak is just above the conduction band minimum. Especially for SO<sub>3</sub> the S DOS distributes widely in the conduction band, which should be responsible for the largest adsorption energy among the three adsorption cases. The adsorption energy closed to 1 eV is an ideal binding for the efficient and reversible gas sensor. However, the adsorption energies of sulfur-based gas molecules on pristine phosphorene are too small for this purpose. The metal decoration can improve the adsorption of gas molecules, so we will discuss the metal decorations and the sulfur-based gas molecule adsorptions on metal decorated phosphorenes.

### 3.2 Sulfur-based gas molecules adsorption on bP-M

The theoretical studies have shown that metal decoration can significantly influence the electronic properties of phosphorene [41]. As well-known to all, if the binding energy of metal on two dimensional (2D) materials is larger than its bulk cohesive energy ( $E_{\text{coh}}$ ), it is going to cluster on the surface of 2D materials. Therefore, to enhance the adsorption of sulfur-based gas molecules on phosphorenes and avert clustering of metal atoms on the surface, eleven metals (Li, Na, K, Rb, Cs, Ca, Sr, Ba, Ni, La, Tl) have been opted to decorate the phosphorene on the basis of  $E_{\text{ads}}/E_{\text{coh}} > 1$  [42]. Here, the electronic properties of metal decorated phosphorenes (bP-Ms) are discussed first to contrast before and after sulfur-based gas molecule adsorptions. Figure 2 shows the band structures and projected density of states (PDOSs) of the bP-Ms. Except for Ni, the outermost *s*-states of alkali metals (AMs = Li, Na, K, Rb, Cs) and those of alkaline earth metals (AEMs = Ca, Sr, Ba), the 6 *p*-state of Tl and 5 *d*-state of La are mainly distributed in the conduction band of phosphorenes, which cause valence-electron transfer from metals to phosphorenes, and thus the Fermi levels shift up in energy. For AM decorated and Tl decorated phosphorenes (bP-AMs and bP-Tl), the Fermi levels shift upward into the conduction bands of phosphorenes and the corresponding bP-AMs and bP-Tl show metal properties. The *s*-states of AMs and *p*-state of Tl are far above the lowest conduction bands of phosphorenes. Unlike the AMs and Tl, the *s*-states of AEMs or *d*-state of La are aligned to the lowest conduction band of phosphorene, which causes the strongly repulsive interaction between metal atomic states and the lowest conduction bands of phosphorenes, so the lowest conduction bands are pushed down. As a consequence, there are large separations between the lowest and second lowest conduction bands for AEM decorated phosphorenes (bP-AEMs) and bP-La. On the other hand, the more *s*- and *d*-electrons transfer for bP-AEMs and bP-La, the more energies shift for Fermi levels. The Fermi levels of bP-AEMs and bP-La are located between about the lowest and second lowest conduction bands. The bP-Ca, bP-Sr and bP-La show semiconductor properties, while bP-Ba shows metal property due to that the Fermi level cross slightly through the second lowest conduction band of phosphorene. Additionally, bP-La has spin-polarized LDOS, as shown in figure 2, with magnetic moment of 1 . For Ni decorated case, the *s*- and *d*-states are distributed in valence band of phosphorene, and the semiconductor property of bP-Ni is remained. However, the bandgap of bP-Ni decreases to 0.769 eV as compared with that of pristine phosphorene, which may be ascribed to the strong hybridized interaction between Ni *d*-state and valence band of phosphorene, and thus the highest valence band is pushed upward.

#### 3.2.1 H<sub>2</sub>S gas molecules adsorption on bP-M

For the H<sub>2</sub>S adsorption on bP-M (M = Li, Na, K, Rb, Cs, Ca, Sr, Ba, Ni, La, Tl), the various initial configurations are considered and are fully optimized. By comparing the adsorption energies, the most stable structures, namely the structures with the largest absolute values of adsorption energies, are achieved as shown in figure 3. In all the structures, the distances between the sulfur and metal atoms are apparently nearer than those between H and metal atoms. Except for bP-Li, bP-Ba and bP-La systems, H<sub>2</sub>S is adsorbed on the bP-M in parallel to the surface of phosphorene. The adsorption energies of H<sub>2</sub>S, the charge transfer amounts and adsorption distances ( $D_{\text{Sub-Gas}}$ )

between sulfur-based gas molecules and substrates are summarized in table 1. As compared with the adsorption energy of 0.220 eV for H<sub>2</sub>S on pristine phosphorene, except for Cs and Tl atoms, the decorations of the rest metals enhance the adsorption of phosphorene to H<sub>2</sub>S molecules. Especially, the adsorption energy of H<sub>2</sub>S molecules on bP-Ni is up to 1.158 eV (see table 1), which is the largest value for all the H<sub>2</sub>S adsorption systems. Correspondingly, the adsorption distance between Ni and S atoms is the smallest among the adsorption of H<sub>2</sub>S on the metal decorated phosphorene, and the value is 2.207 Å. However, the adsorption energies of H<sub>2</sub>S on bP-Tl and bP-Cs are the smallest, even smaller than that on pristine phosphorene. The H<sub>2</sub>S molecules on bP-Tl and bP-Cs have the largest adsorption distance of 3.795 and 3.844 Å respectively, which may be due to the large atomic Tl atom.

Table 1. The adsorption energies ( $E_{ad}$ ) of sulfur-based gas molecules on phosphorene and bP-M. The charge transfer amounts ( $\Delta Q$ ) and adsorption distances ( $D_{Sub-Gas}$ ) between sulfur-based gas molecules and substrates. Positive  $\Delta Q$  denote transferring from sulfur-based gas molecules to phosphorene and bP-M substrates.

Metal	$E_{ad}$ (eV)			$\Delta Q$ (e)			$D_{Sub-Gas}$ (Å)		
	H <sub>2</sub> S	SO <sub>2</sub>	SO <sub>3</sub>	H <sub>2</sub> S	SO <sub>2</sub>	SO <sub>3</sub>	H <sub>2</sub> S	SO <sub>2</sub>	SO <sub>3</sub>
bP	0.220	0.396	0.646	-0.003	-0.182	-0.451	2.818	2.984	2.572
Li	0.695	1.213	1.684	-0.080	-0.626	-1.004	2.484	2.003	1.952
Na	0.441	1.121	1.208	-0.011	-0.523	-0.806	2.875	2.374	2.286
K	0.287	0.945	0.979	0.026	-0.422	-0.674	3.399	2.799	2.673
Rb	0.251	0.949	0.716	0.022	-0.449	-0.526	3.610	2.978	2.640
Cs	0.208	0.810	0.828	0.019	-0.399	-0.640	3.844	3.182	3.001
Ca	0.584	2.086	3.657	0.014	-0.862	-1.416	2.963	2.263	2.147
Sr	0.485	1.929	3.419	0.010	-0.830	-1.435	3.193	2.439	2.295
Ba	0.686	1.657	3.232	-0.059	-0.801	-1.484	3.307	2.633	2.591
Ni	1.158	1.304	1.605	0.042	-0.318	-0.724	2.207	2.074	1.977
La	0.773	2.822	4.508	-0.044	-1.157	-1.325	3.136	2.272	2.175
Tl	0.136	0.597	1.273	0.021	-0.418	-0.832	3.795	2.978	2.721

To understand the internal mechanism of adsorption-energy enhancement and the effect of H<sub>2</sub>S on the electronic and magnetic properties of bP-AM, the LDOSs of the adsorption systems were calculated, as shown in figure 4. The magnetic moment of bP-La reduces slightly from 1.00 to 0.98 after H<sub>2</sub>S adsorption, while those of the other bP-Ms systems remain zero, which are corroborated by the spin asymmetric LDOS for H<sub>2</sub>S adsorption on bP-La case and the spin symmetric LDOSs for H<sub>2</sub>S adsorption on the other bP-M systems. Except for Sr and La decorated cases, the adsorptions of H<sub>2</sub>S have no effect on the electronic properties of the rest bP-M systems. The metal or semiconductor properties of the rest bP-M systems remained after H<sub>2</sub>S adsorption. BP-Sr experiences the semiconductor-to-metal transition, while bP-La experiences the semiconductor-to-half-metal transition. As shown in figure 4, there are the overlap peaks between the sulfur and metal atoms located near -5 or -4 eV for AMs, AEMs and La decorated cases, which should be the reason of improving the adsorption of H<sub>2</sub>S gas molecules. The smallest adsorption energies for Cs

and Tl decorated may be mainly attributed to the large radii of Cs and Tl atoms. For Ni decorated case, the apparent overlap peaks of S and Ni atoms near -6, -4 and -1 eV, implying strong hybridized interaction between H<sub>2</sub>S and bP-Ni substrate, which may be mainly responsible for the largest adsorption energy. Additionally, the states of S and H atoms are far from the Fermi level, implying that H<sub>2</sub>S adsorption almost has no effect on the band structures near it for bP-Ms. Thus, the conductivity properties of bP-Ms are not changed by H<sub>2</sub>S adsorption except for Sr and La decorated cases. For Sr decorated case, the state of H<sub>2</sub>S molecule in conduction band pushes slightly the conduction band minimum of bP-Sr down, which makes the small bandgap (0.07 eV) of bP-Sr disappear. For La decorated case, the charge transfer from substrate to H<sub>2</sub>S makes the Fermi level shift down in energy after H<sub>2</sub>S adsorption, and finally the Fermi level crosses through the spin-up band [see the red curve below the Fermi level in figure 2(j)], which leads to the half-metal property of bP-La.

### 3.2.2 SO<sub>2</sub> gas molecules adsorption on bP-M

For the SO<sub>2</sub> gas adsorption on bP-M, the most stable structures are illustrated in figure 5. Except for SO<sub>2</sub> adsorption on bP-Ni system, the SO<sub>2</sub> preferably adsorbs the bP-AMs with the bond angles toward the metal atoms, and the oxygens of SO<sub>2</sub> are the nearest atoms to the metal atoms. As shown in table 1, all the metal decorations can significantly improve the adsorption capacity of phosphorene to SO<sub>2</sub> gas molecules. The corresponding adsorption energies are ranging from 0.597 eV to 2.822 eV, and all of them are larger than the pristine phosphorene case of 0.396 eV. In addition, we can see that the decoration of AEMs (Ca, Sr, Ba) is more effective than AMs (Li, Na, K, Rb, Cs) for adsorption of SO<sub>2</sub> gas molecules due to larger adsorption energies (see table 1), and that in the same group elements the adsorption energies decrease with the atomic number. As we know, the more charge transfer means the stronger interaction and thus the larger adsorption energy. Consequently, the more valence electrons of AEMs and thus the more electron transfers should be in charge of their larger adsorption energies. On the other hand, short adsorption distance is beneficial for the charge transfer. Thus an increasing adsorption distance should be responsible for decreasing adsorption energies in the same group elements. Adsorption distance may be attributed to the atomic radius increasing with atomic number.

To understand how the SO<sub>2</sub> molecules effect on the properties of the metal decorated substrates, the LDOSs of all SO<sub>2</sub> adsorption systems were calculated and shown in figure 6. The non-zero LDOSs at the Fermi level imply the metal properties for SO<sub>2</sub> adsorptions on bP-AM, bP-AEM, bP-La and bP-Tl systems, while the zero LDOSs at the Fermi level imply semiconductor properties for that on bP-Ni system. Except for bP-Ni, almost all the bP-Ms exhibit spin asymmetry after SO<sub>2</sub> adsorption. The SO<sub>2</sub> adsorbed bP-La has a negligible magnetic moment of 0.0002 μ<sub>B</sub>, on the spin polarization of bP-La system is suppressed by the SO<sub>2</sub> adsorption. Thus, the bP-AMs, bP-AEMs and bP-Tl perceive magnetization on SO<sub>2</sub> adsorption, while bP-La loses the magnetization. In addition, the bP-Ca, bP-Sr and bP-La become metallic, on upward movement of the lowest conduction band of phosphorene (see figure S6 in supporting materials). In fact, upward movements of the lowest conduction bands exist in all the SO<sub>2</sub> adsorbed bP-M systems, including the SO<sub>2</sub> adsorption on bP-AM, bP-Ba and bP-Tl systems (although their metal properties remained), which may be attributed to that the SO<sub>2</sub> adsorptions weaken the interactions between the metals and phosphorenes. For SO<sub>2</sub> adsorption on bP-Ni, upward movement of the lowest conduction band results in that the bandgap of bP-Ni rises from 0.769 to 0.876 eV after SO<sub>2</sub> adsorption. On the other hand, as compared with before SO<sub>2</sub> adsorption, the electron transfers from bP-M systems to SO<sub>2</sub> lead to downward shifts of the Fermi levels for bP-M systems, which may be ascribed to the greater electronegativity of S and O atoms. Except for Ni decorated case, the peaks of O states appear near the Fermi levels, which will introduce the flat bands into the band structures for SO<sub>2</sub> adsorption on bP-Ms (see figure S6). As compared with SO<sub>2</sub> adsorption on the AM systems, the coupling peaks between SO<sub>2</sub> and AEMs are more widely distributed, especially in the conduction band (see figure 6), which may be a reason of more effectively improving the SO<sub>2</sub>

adsorption on phosphorene for the AEM decorated cases. Strong hybridized interaction between the states of  $\text{SO}_2$  molecules and La at -0.8 eV in figure 6(j) can unravel the maximal adsorption energy of 2.822 eV for  $\text{SO}_2$  adsorption on bP-La.

### 3.2.3 $\text{SO}_3$ gas molecules adsorption on bP-M

Optimized structures of  $\text{SO}_3$  adsorption on bP-Ms in different initial configurations are shown in figure 7. As compared with  $\text{H}_2\text{S}$  and  $\text{SO}_2$ , the most stable adsorption configurations of  $\text{SO}_3$  on bP-M are more diverse and have larger adsorption energy for the same metal decorated substrate. However, in all the adsorption configurations of  $\text{SO}_3$  on bP-Ms, the O in  $\text{SO}_3$  is the nearest to metal atoms. The corresponding adsorption energies, 0.716 eV to 4.508 eV, as shown in table 1, are larger than the values of  $\text{SO}_3$  on pristine phosphorene (0.646 eV). Especially, the adsorption configuration of  $\text{SO}_3$  on bP-Tl is similar to that on pristine phosphorene, but the adsorption energy increases from pristine phosphorene of 0.646 eV to 1.273 eV due to the Tl atomic decoration. Thus, all the metal decorations significantly improve the  $\text{SO}_3$  adsorption on phosphorene. Similar to  $\text{SO}_2$  molecule, the adsorption energies of  $\text{SO}_3$  on bP-AEM are larger than that on bP-AM, indicating that the decorations of AEMs are more efficient than AMs in improving the  $\text{SO}_3$  adsorption on phosphorene. As mentioned before, the more charge transfer signifies the stronger interaction and thus the larger adsorption energy [39]. Consequently, the more valence electrons of AEMs and thus electron transfers should be responsible for their larger adsorption energies. On the other hand, in the same group elements, the adsorption energies decrease with the atomic number in lieu of increasing atomic size. As mentioned before, short adsorption distance is advantageous to the charge transfer [26, 27]. The larger atomic size means the larger adsorption distance and thus the more charge transfer, leading to the larger interaction and the larger adsorption energy. Additionally, from table 1, we can see the electrons transfer from bP-Ms to  $\text{SO}_2$  in all the  $\text{SO}_3$  adsorption on bP-M systems, which may be ascribed to the greater electronegativity of S and O atoms.

Figure 8 shows LDOSs of  $\text{SO}_3$  adsorbed bP-Ms to understand the effects of  $\text{SO}_3$  on the bP-Ms substrates. The LDOSs of bP-AM systems and bP-Tl exhibit significantly spin asymmetry after  $\text{SO}_3$  adsorptions, which are mainly contributed by  $\text{SO}_3$  molecules, indicating that the  $\text{SO}_3$  adsorbed bP-AMs and bP-Tl have the magnetism. The  $\text{SO}_3$  adsorbed bP-AEMs and bP-Ni are of spin symmetry LDOSs, having no magnetism. The magnetic moment of  $\text{SO}_3$  adsorbed bP-La is only 0.0003  $\mu_B$ , which can be ignored and the corresponding LDOS shows almost spin-symmetry. Therefore, the bP-AMs and bP-Tl develop magnetism on  $\text{SO}_3$  adsorptions, while the bP-La adversely loses the magnetism. The  $\text{SO}_3$  adsorbed bP-Li, bP-Na, bP-AEMs, bP-Ni and bP-Tl systems have zero DOSs at the Fermi levels of semiconductor properties. The  $\text{SO}_3$  adsorbed bP-K, bP-Rb, bP-Cs and bP-La have non-zero DOSs at the Fermi levels, implying that they possess metal properties. In contrast to before  $\text{SO}_3$  adsorption, the bP-Li, bP-Na, bP-Ba and bP-Tl experience the metal-to-semiconductor transitions after  $\text{SO}_3$  adsorption, while the bP-La experiences the semiconductor-to-metal transition. As showed in figure S7 of supporting materials, the effect of  $\text{SO}_3$  on the band structures of bP-M systems is the largest among the three gas molecules, which may be due to the largest amount of electron transfer from the bP-Ms substrate to  $\text{SO}_3$  molecules. In addition, the  $\text{SO}_3$  introduces impurity states into/near bandgaps or into the valence bands. Accordingly, the Fermi levels of bP-M systems show different degree of moving down as a result of the charge transfer from the substrates to  $\text{SO}_3$  molecules. As shown in figure 8(a) and (b), the highest spin-up states of  $\text{SO}_3$  molecules for bP-Li and bP-Na systems are respectively located in valence and bandgap, which are both below the Fermi levels. This leads to more electron transfer from bP-Li and bP-Na to  $\text{SO}_3$  molecules and thus bP-Li and bP-Na are restored to semiconductor, which should be responsible for metal-to-semiconductor transitions of bP-Li and bP-Na. But for bP-K, bP-Rb and bP-Cs systems, as shown in figure 8(c)-(e), the highest spin-up  $\text{SO}_3$  states cross through the lowest conduction bands of bP-M, leading to less electrons transfer and thus metal properties being remained. For bP-AEM,

both the highest spin-up and spin-down bands are located near valence band maximum (VBM) and below the Fermi levels, resulting in that the Fermi levels shift down due to electrons transferring from bP-AEM to SO<sub>3</sub> molecules. On the other hand, the interaction between AEM atom and SO<sub>3</sub> molecules weakens that between AEM and phosphorene, and thus the lowest conduction band moves upward and the energy separation between the lowest and the second lowest conduction bands restores to pristine phosphorene case. Consequently, the bP-AEM systems show semiconductor properties after SO<sub>3</sub> adsorptions, and complete the metal-to-semiconductor transitions. For SO<sub>3</sub> adsorbed on bP-Ni system, the bandgap of bP-Ni system increases to 0.882 eV due to the interaction between AEM atoms and SO<sub>3</sub> molecules. The VBM is transferred from X to Y point, and thus the bP-Ni exhibits indirect semiconductor properties and experiences direct-to-indirect transition. For SO<sub>3</sub> adsorbed bP-La system, the metal flat band disappears and thus the lowest conduction band shifts upward owing to the interaction of SO<sub>3</sub> molecule with La atom on phosphorene. This leads to the transition from metal to semiconductor of the bP-Tl system after SO<sub>3</sub> adsorption. This may be ascribed to the SO<sub>3</sub> flat bands in bandgap of bP-Tl, which push upward the lowest conduction band. Compared to the LDOS of SO<sub>3</sub> adsorbed bP-AM systems, the coupling peaks between SO<sub>3</sub> molecules and metals are more widely distributed at -9 eV, -6~-5 eV, -3~0 eV and in the conduction band, which also may be the reason that the AEM decoration more effectively in improving the SO<sub>3</sub> adsorption on phosphorene. For SO<sub>3</sub> adsorbed bP-Ni, bP-La and bP-Tl systems, there are many coupling peaks between the states of metal atoms and SO<sub>3</sub> molecules near the Fermi level, which may be responsible for the large interactions of bP-Ms and SO<sub>3</sub> molecules. As compared with other metal cases, more coupling peaks of La and SO<sub>3</sub> molecules are located in the band, contributing to the excellent adsorption performance of SO<sub>3</sub> molecules on bP-La.

Table 2. The magnetic moment ( $M$ ), bandgap ( $E_g$ ), and direct/indirect bandgap (D/I) of sulfur-based gas molecules on phosphorene and bP-M. The units of  $M$  and  $E_g$  are  $\mu_B$  and eV, respectively.

Metal	bP-M			H <sub>2</sub> S-bP-M			SO <sub>2</sub> -bP-M			SO <sub>3</sub> -bP-M		
	$M$	$E_g$	D/I	$M$	$E_g$	D/I	$M$	$E_g$	D/I	$M$	$E_g$	D/I
Li	0	0		0	0		0.71	0		1.00	0.896/0.493	D/I
Na	0	0		0	0		0.58	0		0.92	0.094/0.839	I
K	0	0		0	0		0.50	0		0.81	0	
Rb	0	0		0	0		0.50	0		0.61	0	
Cs	0	0		0	0		-0.46	0		0.76	0	
Ca	0	0.119	I	0	0.05	I	0.99	0		0	0.710	I
Sr	0	0.071	I	0	0		0.99	0		0	0.626	I
Ba	0	0		0	0		1.00	0		0	0.868	D
Ni	0	0.769	D	0	0.858	D	0	0.876	D	0	0.882	I
La	1.00	0.116/0.299	I	0.98	0/0.210	I	0	0		0	0	
Tl	0			0			0.51			0.99	0.417/0.738	I

The values of magnetization and band gap obtained in the various samples with H<sub>2</sub>S, SO<sub>2</sub> and SO<sub>3</sub> adsorption on phosphorene of various metal decorations are summarized in table 2. As mentioned above, the adsorption energies larger than 1.5 eV are suitable for gas molecule capture or single sensing, whereas the adsorption energies near around

1 eV are ideal bindings for highly efficient and reversible gas sensors. Therefore, from table 1, one can see that the phosphorenes with AEM and La decorations can be served as capturing the SO<sub>2</sub> and SO<sub>3</sub> molecules, and that those with Li and Ni decorations can only be utilized as the SO<sub>3</sub> capture. From table 2, it is observed that the Li, Ca, Sr and Ba decorated phosphorenes can be used as selective single sensing for SO<sub>3</sub> on the basis of increase of bandgap and thus decrease of conductivity after SO<sub>3</sub> adsorption. The adsorption energies of H<sub>2</sub>S on K, Rb, Cs and Tl decorated phosphorenes are so small that H<sub>2</sub>S gases are easy to dissociate from substrates, and thus the K, Rb, Cs and Tl decorated phosphorenes are not suitable for H<sub>2</sub>S sensing. In addition to the moderate adsorption energy, the change in measurable property is necessary for reversible gas sensors. Therefore, the Tl decorated phosphorene is promising to be a selective reversible SO<sub>3</sub> sensor due to the metal-to-semiconductor transition after gas molecule adsorption, while the semiconductor-to-half-metal transition of the La decorated phosphorene makes it be the potential candidate as a selective reversible H<sub>2</sub>S sensor. Interestingly, it is found that the magnetic moments are positive and negative, respectively, after SO<sub>2</sub> and SO<sub>3</sub> adsorptions, which may be a basis for selectively sensing the SO<sub>2</sub> or SO<sub>3</sub> gas molecules.

## 4. Conclusion

In summary, the adsorption of H<sub>2</sub>S, SO<sub>2</sub> and SO<sub>3</sub> on various metal-decorated phosphorene have been systematically investigated by using DFT. Eleven metals (Li, Na, K, Rb, Cs, Ca, Sr, Ba, Ni, La, Tl),  $E_{\text{ads}}/E_{\text{coh}} > 1$ , are considered. Except for H<sub>2</sub>S on bP-Tl, the results show that the decoration of metals can significantly improve the adsorption of phosphorene to sulfur-based gas molecules, and the order of adsorption capacity is La > AEM > AM. In the analysis of LDOSs, it is found that the phosphorenes with Sr and La decorations undergo the transitions from semiconductor to metal and from semiconductor to half-metal after H<sub>2</sub>S adsorption. The AM, AEM and Tl decorated phosphorenes undergo non-magnetic-to-magnetic transitions, after SO<sub>2</sub> adsorption, while the La decorated phosphorene undergoes magnetic-to-non-magnetic transition. Meantime, the Ca, Sr and La decorated phosphorenes also have transition from semiconductor to metal after SO<sub>2</sub> adsorption. For SO<sub>3</sub> adsorption cases, the AM and Tl decorated phosphorenes obtain non-magnetic-to-magnetic transitions, while the La decorated phosphorene perceive the transition from magnetic to non-magnetic. The Li, Na and AEM decorated phosphorenes experience the transitions from metal to semiconductor, while the La decorated phosphorene experiences semiconductor-to-metal transition. On the basis of the criterion of adsorption energy around 1 eV and the changes in properties, the phosphorenes with La and Tl decorations are promising selective reversible sensors for H<sub>2</sub>S and SO<sub>3</sub> detections, respectively. According to whether the magnetic moment is positive or negative, the Cs decorated phosphorene could be a potential selective reversible sensor for SO<sub>3</sub> or SO<sub>2</sub> detection.

## Declarations

### Conflicts of interest

There are no conflicts to declare.

### Acknowledgments

This work was supported by the National Natural Science Foundation of China (Nos. 11774052, 11774051, 61771137, 11674053), the National Basic Research Program of China (No. 2015CB352100), and the National Science Foundation

of Jiangsu Province of China (No. BK20171355). Additionally, we acknowledge the Shanghai Supercomputer Center and Big Data Center of Southeast University for the facility support on the calculations in this manuscript.

## References

- [1] Zeng Y., Zhang K., Wang X. L., Sui Y., Zou B., Zheng W. T., Zou G.T. Rapid and selective H<sub>2</sub>S detection of hierarchical ZnSnO<sub>3</sub> nanocages. *Sensor. Actuator. B***159**, 245-250 (2011).
- [2] Bari R. H., Patil P. P., Patil S. B., Bari A. R. Detection of H<sub>2</sub>S gas at lower operating temperature using sprayed nanostructured In<sub>2</sub>O<sub>3</sub> thin films. *Bull. Mater. Sci.***36**, 967-972 (2013).
- [3] Guo Y. Y., Li Y., Zhu T. Y., Ye M. Investigation of SO<sub>2</sub> and NO adsorption species on activated carbon and the mechanism of NO promotion effect on SO<sub>2</sub>. *Fuel***143**, 536-542 (2015).
- [4] Chatterjee C., Sen A. Sensitive colorimetric sensors for visual detection of carbon dioxide and sulfur dioxide. *J. Mater. Chem.* **A3**, 5642-5647 (2015).
- [5] Klimont Z., Smith S. J., Cofala J. The last decade of global anthropogenic sulfur dioxide: 2000–2011 emissions. *Environ. Res. Lett.* **8**, 014003 (2013).
- [6] Robinson E., Robbins R. C. Gaseous sulfur pollutants from urban and natural sources. *J. Air Pollut. Cont. Assn.***29**, 164-165 (1979).
- [7] Khan M. A. H., Rao M. V., Li Q. Recent advances in electrochemical sensors for detecting toxic gases: NO<sub>2</sub>, SO<sub>2</sub> and H<sub>2</sub>S. *Sensors***19**, 905 (2019).
- [8] Kampa M., Castanas E. Human health effects of air pollution. *Environ. Pollution***151**, 362-367 (2008).
- [9] Kikuchi R. Environmental management of sulfur trioxide emission: Impact of SO<sub>3</sub> on human health. *Environ. Management***27**, 837–844 (2001).
- [10] Khan R. R., Siddiqui M. J. A. Review on effects of particulates, sulfur dioxide and nitrogen dioxide on human health. *Int. Res. J. Environment Sci.***3**, 70-73 (2014).
- [11] Selene C. H., Chou J. Hydrogen sulfide: Human health aspects. *Concise International Chemical Assessment Document***53**, (2003).
- [12] Solomon D., Zhao F. J., Mcgrath S. P. Atmospheric SO<sub>2</sub> emissions since the late 1800s change organic sulfur forms in humic substance extracts of soils, *Environ. Sci. Technol.* **42**, 3550-3555 (2008).
- [13] Yu Q., Zhang T., Ma X., Kang R., Mulder J., Larssen T., Duan L. Monitoring effect of SO<sub>2</sub> emission abatement on recovery of acidified soil and streamwater in southwest china. *Environ. Sci. Technol.***51**, 9498–9506 (2017).
- [14] Smirnov M. Y., Kalinkin A. V., Pashis A. V., Prosvirin I. P., Bukhtiyarov V. I. Interaction of SO<sub>2</sub> with Pt model supported catalysts studied by XPS. *J. Phys. Chem. C***118**, 22120-22135 (2014).
- [15] Li H. L., Wu C. Y., Li Y., Li L. Q., Zhao Y., Zhang J. Y. Impact of SO<sub>2</sub> on elemental mercury oxidation over CeO<sub>2</sub>–TiO<sub>2</sub> catalyt. *Chem. Eng. J.* **219**, 319-326 (2013).

- [16] Machida M., Kawada T., Yamashita H., Tajiri T. Role of oxygen vacancies in catalytic SO<sub>3</sub> decomposition over Cu<sub>2</sub>V<sub>2</sub>O<sub>7</sub> in solar thermochemical water splitting cycles. *J. Phys. Chem. C* **117**, 26710-26715 (2013).
- [17] Ye H., Liu L., Xu Y., Wang L., Chen X., Zhang K., Liu Y., Koh S. W., Zhang G. SnSe monolayer: A promising candidate of SO<sub>2</sub> sensor with high adsorption quantity. *Appl. Surf. Sci.* **484**, 33-38 (2019).
- [18] Esrafil M. D., Saeidi N. *et al.* A DFT study on SO<sub>3</sub> capture and activation over Si- or Al-doped graphene. *Chem. Phys. Lett.* **658**, 146-151 (2016).
- [19] Novoselov K. S., Geim A. K., Morozov S. V., Jiang D., Zhang Y., Dubonos S. V., Grigorieva I. V., Firsov A. A. Electric field effect in atomically thin carbon films. *Science* **306**, 666-669 (2004).
- [20] Geim A. K., Novoselov, K. S. The rise of graphene. *Nat. Mater.* **6**, 183-191 (2007).
- [21] Dean C. R., Young A. F., Meric I., Lee C., Wang L., Sorgenfrei S., Watanabe K., Taniguchi T., Kim P., Shepard K. L., Hone J. Boron nitride substrates for high-quality graphene electronics. *Nat. Nanotechnol.* **5**, 722-726 (2010).
- [22] Mak K. F., Lee C., Hone J., Shan J., Heinz T. F. Atomically thin MoS<sub>2</sub>: A new direct-gap semiconductor. *Phys. Rev. Lett.* **105**, 136805 (2010).
- [23] Chhowalla M., Shin H. S., Eda G., Li L. J., Loh K. P., Zhang H. The chemistry of two-dimensional layered transition metal dichalcogenide nanosheets. *Nat. Chem.* **5**, 263-275 (2013).
- [24] Xu X. D., Yao W., Xiao D., Heinz T. F. Spin and pseudospins in layered transition metal dichalcogenides. *Nat. Phys.* **10**, 343-350 (2014).
- [25] Leenaerts O., Partoens B., Peeters F. M. Adsorption of H<sub>2</sub>O, NH<sub>3</sub>, CO, NO<sub>2</sub> and NO on graphene: A first-principles study. *Phys. Rev. B* **77**, 125416 (2018).
- [26] Cai Y. Q., Ke Q. Q., Zhang G., Zhang Y. W. Energetics, charge Transfer and magnetism of small molecules physisorbed on phosphorene. *J. Phys. Chem. C* **119**, 3102-3110 (2015).
- [27] Kou L., Frauenheim T., Chen C. F. Phosphorene as a superior gas sensor: Selective adsorption and distinct I-V response, *J. Phys. Chem. Lett.* **5**, 2675-2681 (2014).
- [28] Abbas A. N., Liu B., Chen L., Ma Y., Cong S., Aroonyadet N., Kopf M., Nilges T., Zhou C. Black phosphorus gas sensors. *ACS Nano* **9**, 5618-5624 (2015).
- [29] Kuang A., Kuang M. Q., Yuan H. K., Wang G. Z., Chen H., Yang X. L. Acidic gases (CO<sub>2</sub>, NO<sub>2</sub> and SO<sub>2</sub>) capture and dissociation on metal decorated phosphorene. *Appl. Surf. Sci.* **410**, 505-512 (2017).
- [30] Lalitha M., Nataraj Y., Lakshmipathi S. C decorated and doped phosphorene for gas adsorption. *App. Surf. Sci.* **377**, 311-323 (2016).
- [31] Lei S. Y., Guo S. J., Sun X. L., Yu H., Xu F., Wan N., Wang Z. Capture and dissociation of dichloromethane on Fe, Ni, Pd and Pt decorated phosphorene. *Appl. Surf. Sci.* **495**, 143533 (2019).
- [32] Kaewmaraya T., Ngamwongwan L., Moontragoon P., Karton A., Hussain T. Drastic improvement in gas-sensing characteristics of phosphorene nanosheets under vacancy defects and elemental functionalization. *J. Phys. Chem. C* **122**, 20186-20193 (2018).

- [33] Kresse G., Furthmüller J. Efficiency of ab-initio total energy calculations for metals and semiconductors using a plane-wave basis set. *Comput. Mater. Sci.* **6**, 15-50 (1996).
- [34] Kresse G., Furthmüller J. Efficient iterative schemes for ab initio total-energy calculations using a plane-wave basis set. *Phys. Rev. B* **54**, 11169-1118 (1996).
- [35] Perdew J. P., Burke K., Ernzerhof M. Generalized gradient approximation made simple. *Phys. Rev. Lett.* **77**, 3865-3868 (1996).
- [36] Grimme S. Semiempirical GGA-type density functional constructed with a long-range dispersion correction. *J. Comput. Chem.* **27**, 1787-1799 (2006).
- [37] Li Q. F., Duan C. G., Wan X. G., Kuo J. L. Theoretical prediction of anode materials in Li-ion batteries on layered black and blue phosphorus. *J. Phys. Chem. C* **119**, 8662-8670 (2015).
- [38] Li X. B., Guo P., Cao T. F., Liu H., Lau W. M., Liu L.M. Structures, stabilities and electronic properties of defects in monolayer black phosphorus. *Sci. Rep.* **5**, 10848 (2015).
- [39] Hussain T., Kaewmaraya T., Chakraborty S., Vovusha H., Amornkitbamrung V., Ahuja R. Defected and functionalized germanene-based nanosensors under sulfur comprising gas exposure. *ACS Sens.* **3**, 867–874 (2018).
- [40] Ienco A., Manca G., Peruzzini M., Mealli C. Modelling strategies for the covalent. *Dalton Trans.* **47**, 17243–17256 (2018).
- [41] Ding Y., Wang Y. L. Structural, electronic and magnetic properties of adatom adsorptions on black and blue phosphorene: A first-principles study. *J. Phys. Chem. C* **119**, 10610-10622 (2015).
- [42] Lei S.Y., Shen H.Y., Sun Y.Y., Wan N., Yu H., Zhang S.B. Enhancing the ambient stability of few-layer black phosphorus by surface modification. *RSC Adv.* **8**, 14676-14683 (2018).

## Figures

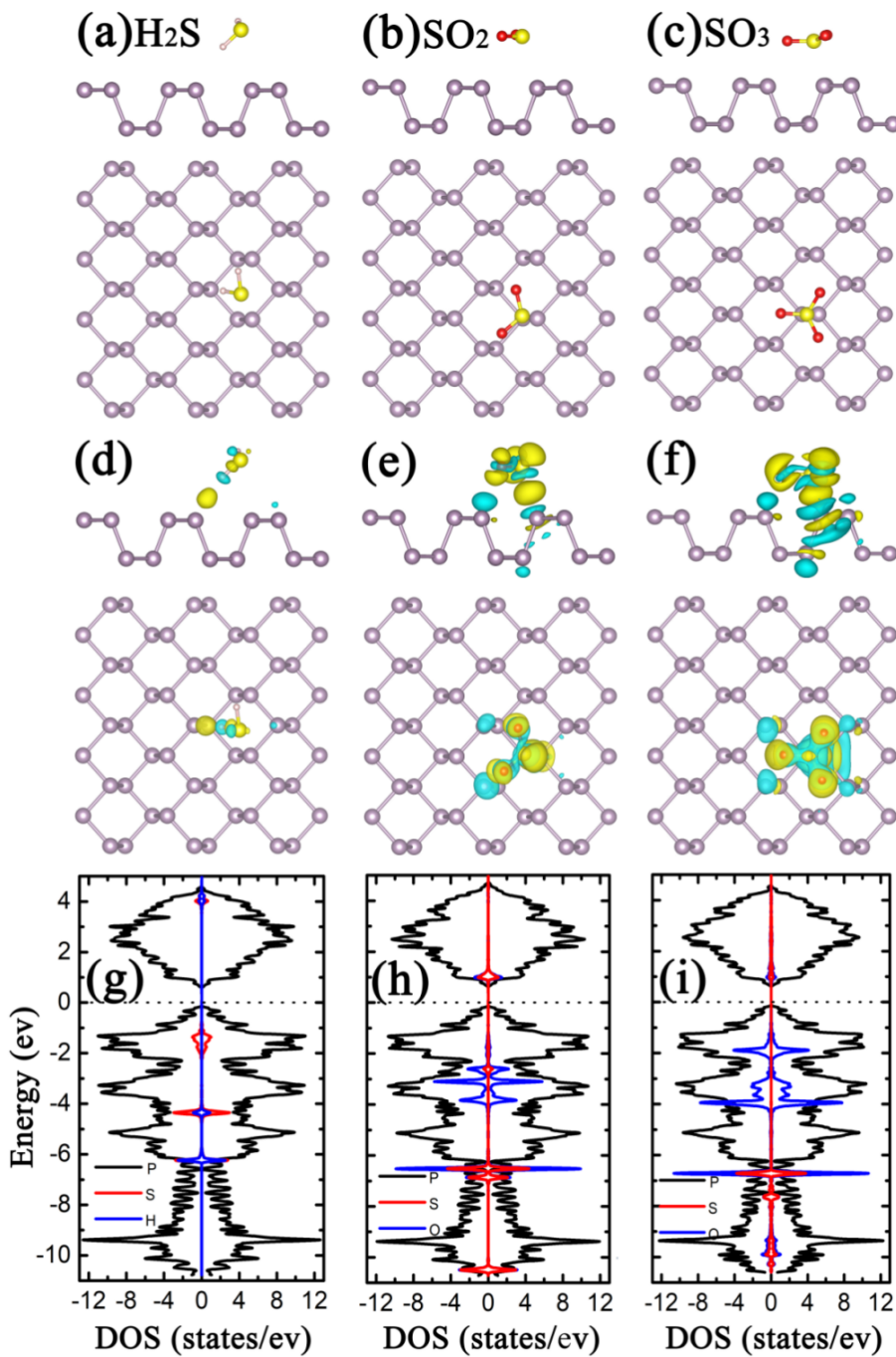


**Figure 1**

The optimized structure of (a) H<sub>2</sub>S, (b) SO<sub>2</sub> and (c) SO<sub>3</sub> adsorbed on 3×4 pristine phosphorene, (d), (e) and (f) the DCD corresponding to (a), (b) and (c), respectively, (g), (h) and (i) the LDOS corresponding to (a), (b) and (c), respectively. Purple, yellow, pink, and red balls in (a)~(f) represent P, S, H and O atoms, respectively. Yellow and blue regions in (d)~(f) denote charge accumulation and charge depletion, respectively. The black, red and blue curves in (g)~(i) represent respectively the LDOS of P, S and H (O), and set the Fermi level to zero.

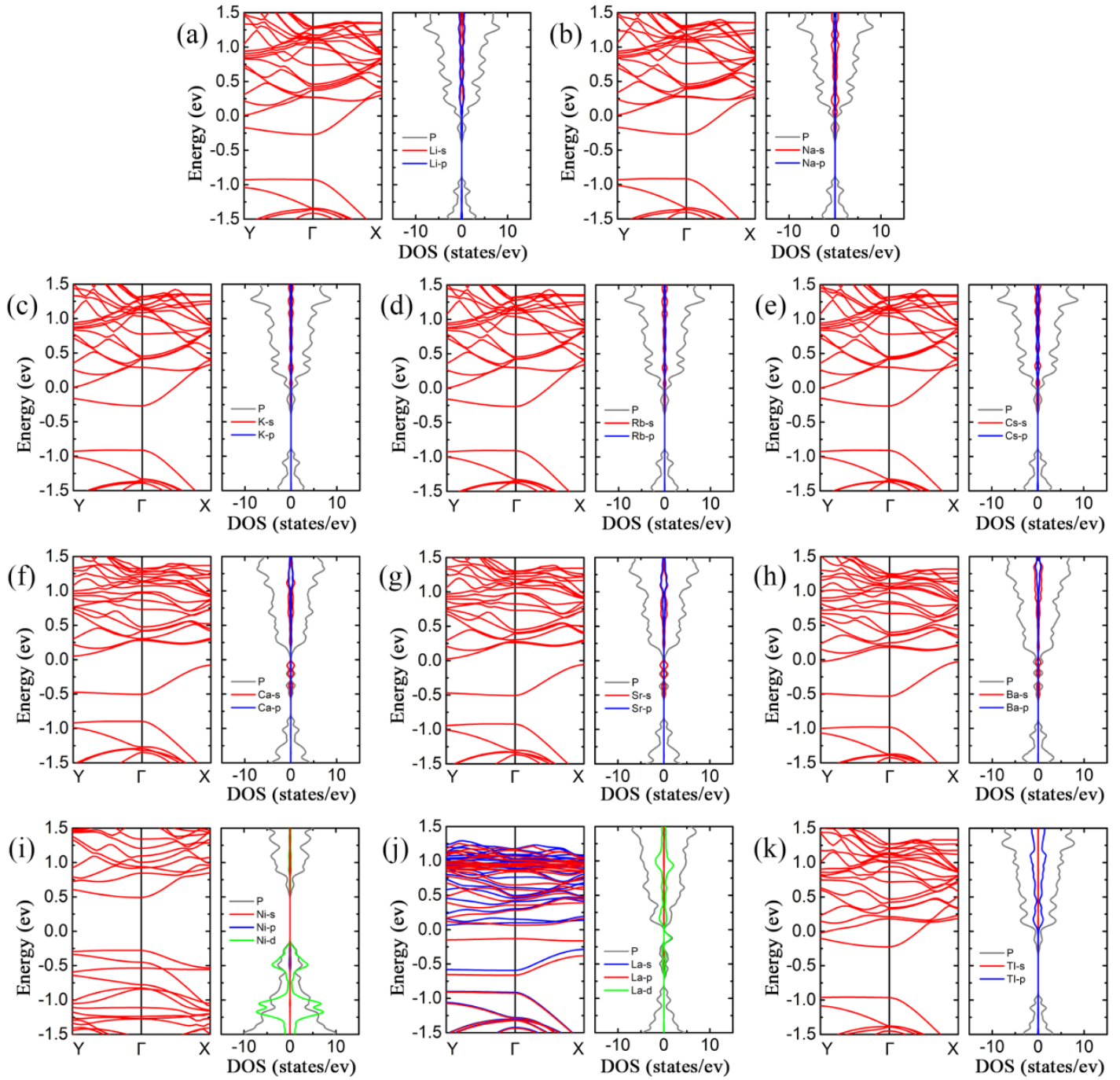


**Figure 2**

The band structures and projected DOSs of (a) bP-Li, (b) bP-Na, (c) bP-K, (d) bP-Rb, (e) bP-Cs, (f) bP-Ca, (g) bP-Sr, (h) bP-Ba, (i) bP-Ni, (j) bP-La and (k) bP-Tl. The red and blue curves represent the spin-up and spin-down bands, respectively. The gray curves in projected DOS represent state of P, and the red, blue and green curves represent the s-, p- and d-states for metal atoms.

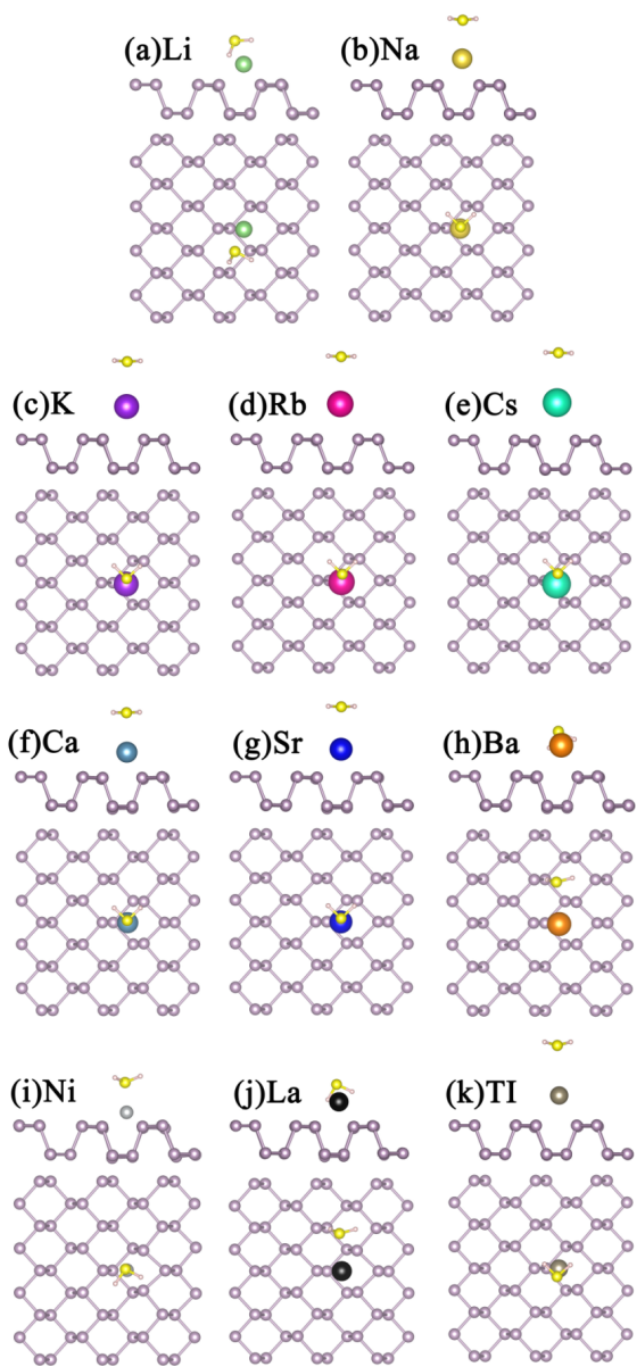


**Figure 3**

The optimized structures of H<sub>2</sub>S adsorption on bP-M (M = Li, Na, K, Rb, Cs, Ca, Sr, Ba, Ni, La, Tl). The Green, gold, purple, red, cyan, dark cyan, blue, orange, light gray, black and gray balls represent respectively Li, Na, K, Rb, Cs, Ca, Sr, Ba, Ni, La and Tl.

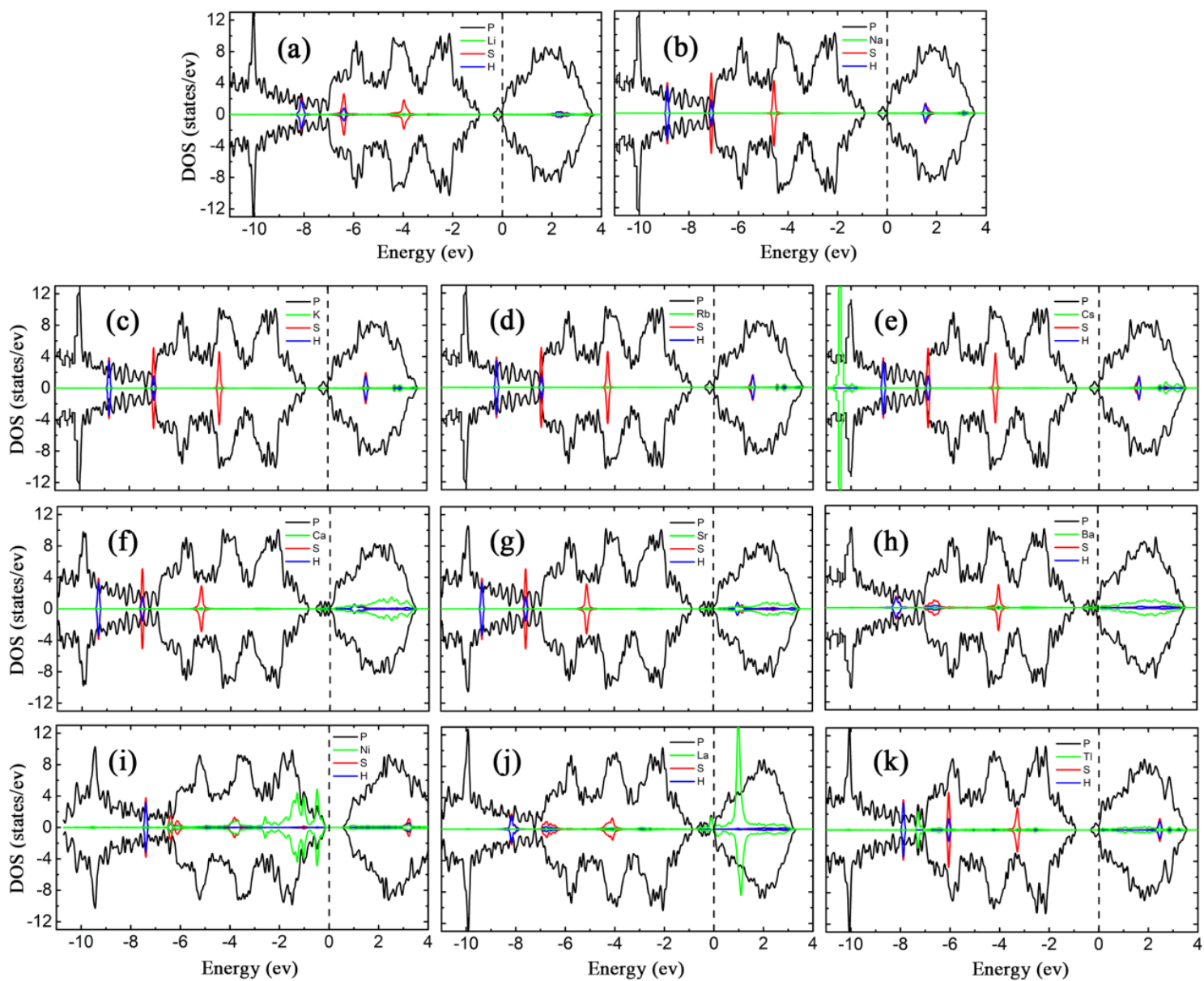


**Figure 4**

The LDOSs of H<sub>2</sub>S adsorption on bP-M (M = Li, Na, K, Rb, Cs, Ca, Sr, Ba, Ni, La, Tl). The black, green, red and blue curves represent the LDOS of P, metal, S and H, respectively. The Fermi level is set to zero.

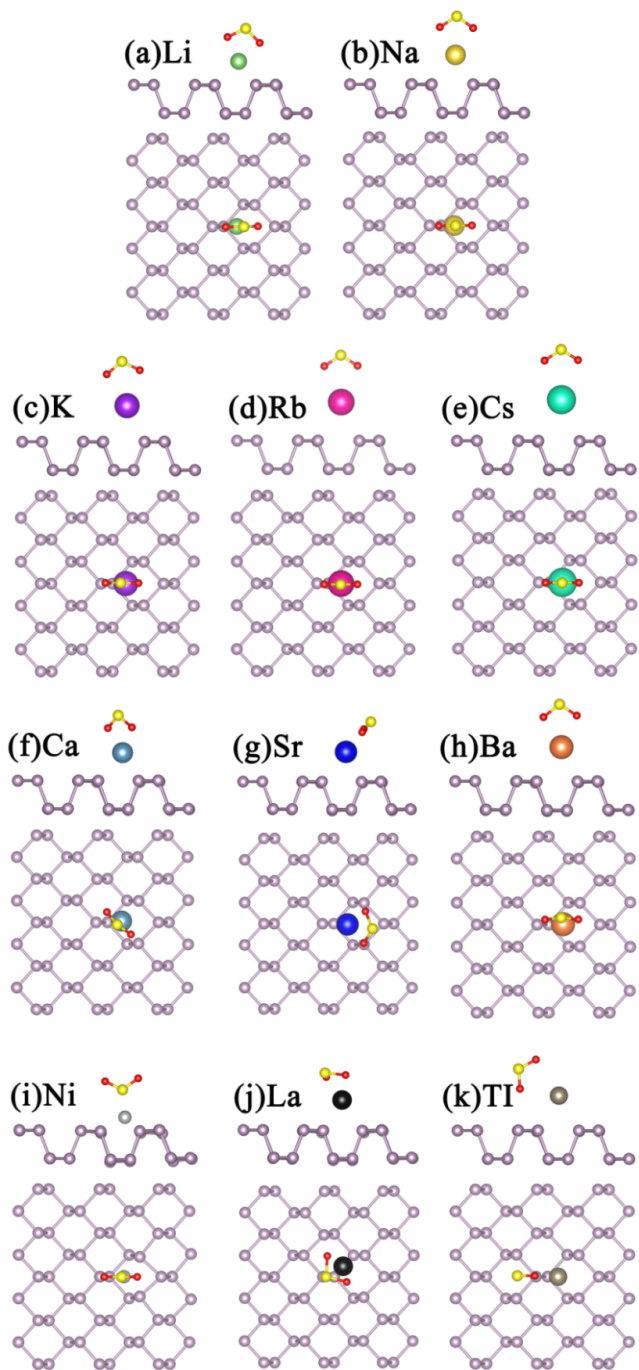


**Figure 5**

The optimized structures of SO<sub>2</sub> adsorbed bP-M (M = Li, Na, K, Rb, Cs, Ca, Sr, Ba, Ni, La, Tl). The green, gold, purple, red, cyan, dark cyan, blue, orange, light gray, black and gray balls represent Li, Na, K, Rb, Cs, Ca, Sr, Ba, Ni, La and Tl, respectively.

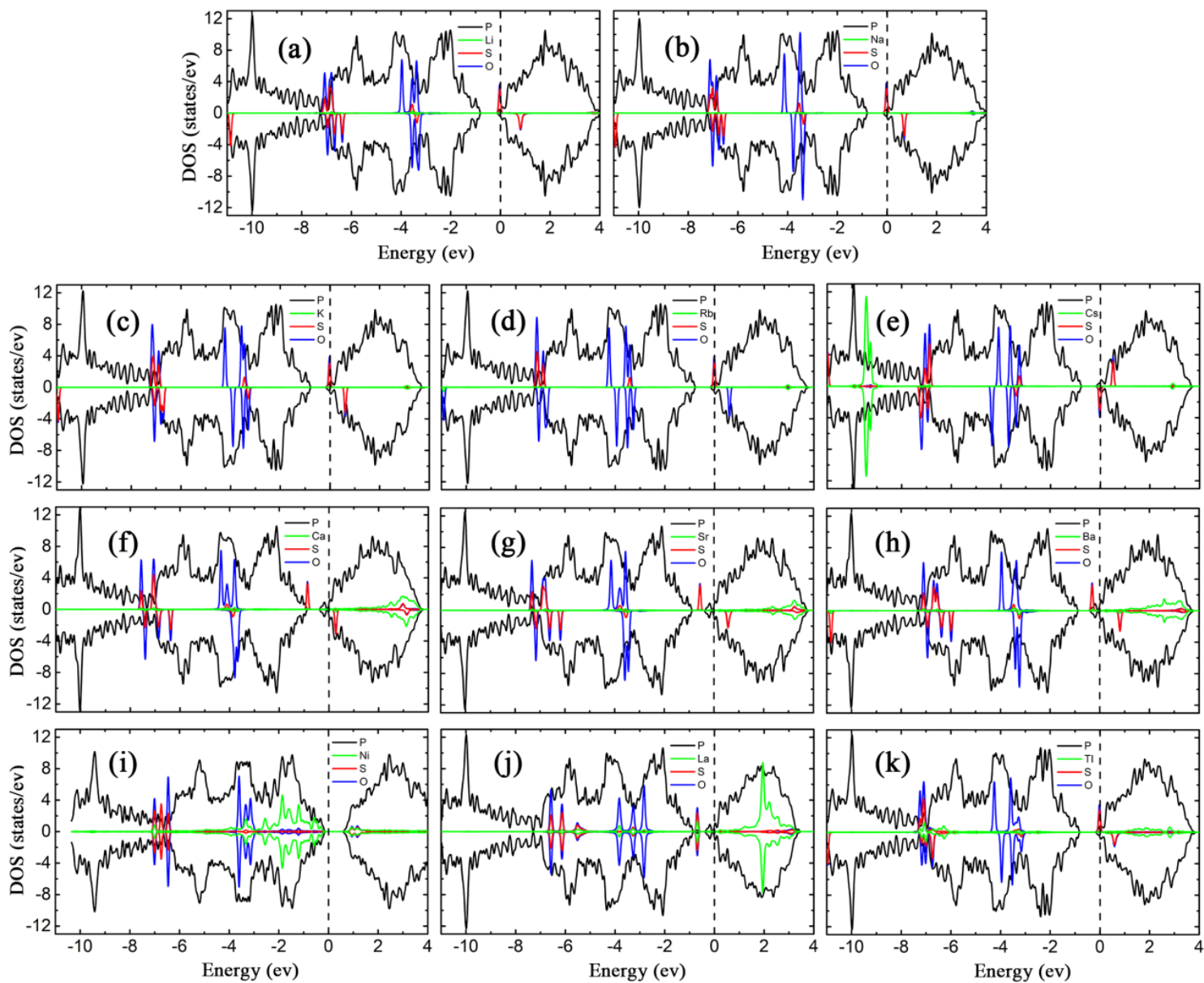


**Figure 6**

The LDOSs of SO<sub>2</sub> adsorption on bP-M (M = Li, Na, K, Rb, Cs, Ca, Sr, Ba, Ni, La, Tl). The black, green, red and blue curves represent the LDOS of P, metal, S and O, respectively. The Fermi level is set to zero.

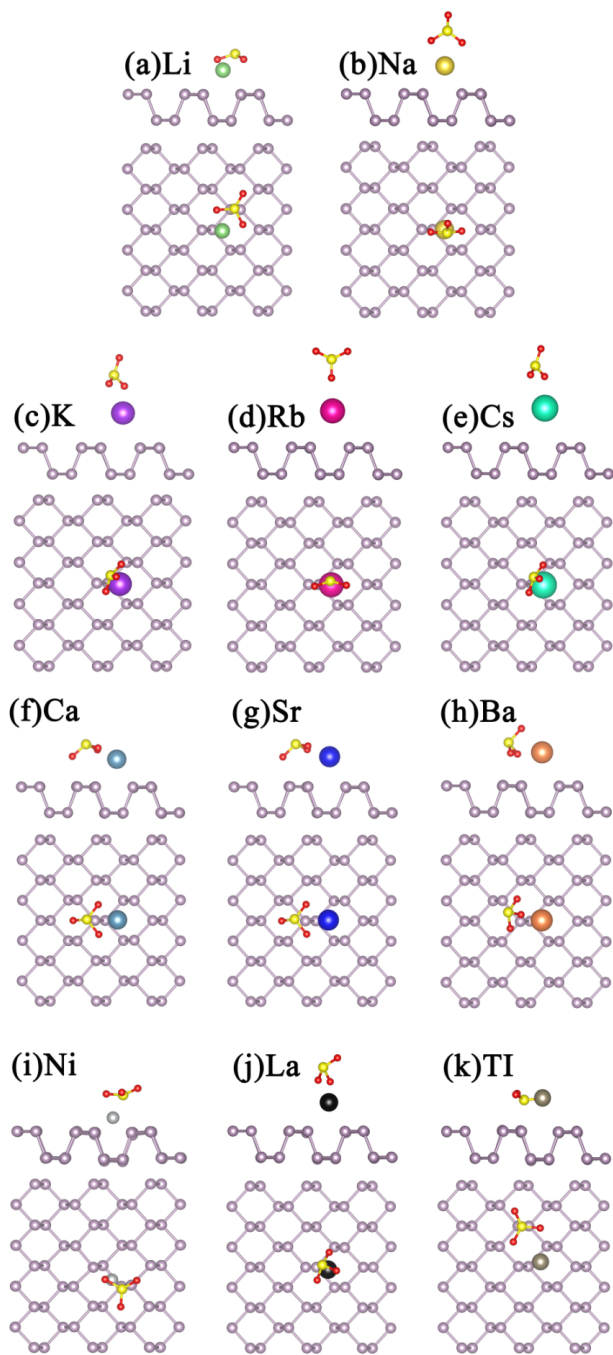


**Figure 7**

The optimized structures of SO<sub>3</sub> adsorption on bP-M (M = Li, Na, K, Rb, Cs, Ca, Sr, Ba, Ni, La, Tl). The green, gold, purple, red, cyan, dark cyan, blue, orange, light gray, black and gray balls represent respectively Li, Na, K, Rb, Cs, Ca, Sr, Ba, Ni, La and Tl, respectively.

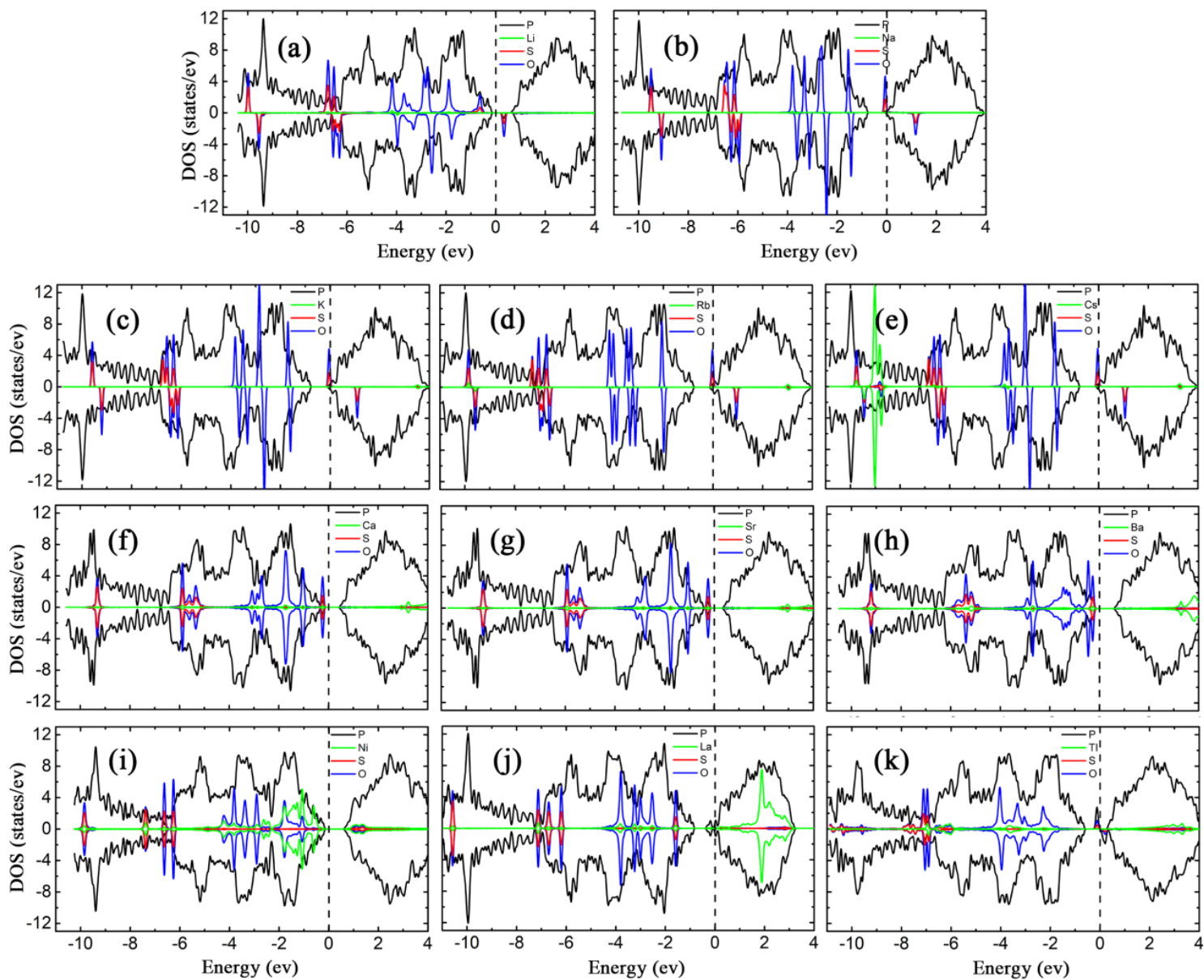


**Figure 8**

The LDOSs of SO<sub>3</sub> adsorption on bP-M (M = Li, Na, K, Rb, Cs, Ca, Sr, Ba, Ni, La, Tl). The black, green, red and blue curves represent the LDOS of P, metal, S and O, respectively. The Fermi level is set to zero.

## Supplementary Files

This is a list of supplementary files associated with this preprint. Click to download.

- [Supplementarymaterial.docx](#)
- [formula.docx](#)